https://doi.org/10.5194/egusphere-2025-5892
Preprint. Discussion started: 6 February 2026

Downstream export dominates the fate of groundwater-derived CO_2 in a boreal stream

Carolina Olid[1*], Demian Hauptmann[2], Jan Karlsson[2], Marcus Klaus[3]

[1]UB-Geomodels Research Institute, Department of Earth and Ocean Dynamics, University of Barcelona, Barcelona, Spain
[2] Department of Ecology, Environment and Geoscience, Umeå University, Umeå, Sweden
[3] Department of Forest Ecology and Management, Swedish University of Agricultural Sciences, Umeå, Sweden

Correspondence to: Carolina Olid (carolina.olid@ub.edu)

https://doi.org/10.5194/egusphere-2025-5892
Preprint. Discussion started: 6 February 2026

Abstract

Groundwater inflow is increasingly recognized as a major source of carbon dioxide (CO_2) to streams. Yet, its fate - whether it is emitted to the atmosphere or exported downstream - remains poorly characterized, partly due to the challenges of quantifying groundwater inflow rates at high spatial (meter) and temporal (days) resolutions. In this study, we assessed the fate of groundwater-derived CO_2 in a 400 m boreal headwater stream reach by combining fine-scale measurements of groundwater inputs, emissions and downstream export of CO_2. Spatial patterns in groundwater-derived CO_2 inputs were primarily driven by the magnitude of groundwater inflows, which were controlled by catchment characteristics, such as stream slope and localized aquifer properties. Temporally, peaks in groundwater CO_2 inputs during snowmelt were primarily driven by increased groundwater discharge rather than elevated CO_2 concentrations in the groundwater, whereas peaks during summer and early autumn were associated with rainfall events and higher CO_2 concentrations in groundwater, likely resulting from enhanced soil respiration. Overall, groundwater CO_2 inputs exceeded CO_2 emissions by up to fourfold, with 40-60% of terrestrial CO_2 transported downstream. This indicates that a substantial portion bypasses immediate atmospheric emission and may contribute to CO_2 emission further along the stream network or be cycled through in–stream processes downstream. Our results demonstrate how and to what extent groundwater inflows contribute to the variability of CO_2 fluxes from headwater streams. These findings highlight the importance of integrative assessments of CO_2 fluxes (i.e. groundwater inputs, emissions, and downstream export), which consider both in-stream processes and catchment-scale dynamics. This is particularly important in the context of climate-driven changes in hydrology and terrestrial carbon cycling.

https://doi.org/10.5194/egusphere-2025-5892
Preprint. Discussion started: 6 February 2026

1 Introduction

Inland waters play a critical role in the emission of carbon dioxide (CO_2) into the atmosphere (Raymond et al., 2013). Global assessments of riverine CO_2 emissions suggest that rivers and streams almost balance out the terrestrial ecosystems' carbon (C) uptake and are of similar magnitude as the net ocean CO_2 uptake from the atmosphere (Drake et al., 2018). Among riverine systems, headwater streams (i.e., first to third-order streams using the Strahler number) are particularly important because they contribute to more than 70% of global riverine CO_2 emission while representing only 17% of river surface area (Li et al., 2021). Yet, despite progress in understanding the role of headwater streams in the global C cycle, uncertainties remain regarding the underlying mechanisms regulating these fluxes.

In the boreal biome, which holds approximately one-third of the Earth's terrestrial C stocks (Bradshaw & Warkentin, 2015), headwater streams are both numerous and characterized by elevated CO_2 concentrations (Rasilo et al., 2017; Wallin et al., 2018). The frequent CO_2 supersaturation observed in these systems has been linked to *in-situ* mineralization of terrestrial organic C (OC), alongside abiotic processes such as weathering and photooxidation (e.g. Rasilo et al., 2017). However, recent attention has increasingly focused on lateral inputs from groundwater, particularly in small streams that are strongly connected to the surrounding soils and groundwater (Duvert et al., 2018; Hotchkiss et al., 2015; Lupon et al., 2019). While much of the CO_2 derived from groundwater is likely to be emitted to the atmosphere when it enters the stream, some fraction may be transported downstream, where it can be emitted or processed via in-stream biogeochemical pathways. While the relative contributions of groundwater and in-stream sources remain unclear, the dual role of groundwater as both a driver of local CO_2 emission and a contributor to downstream C fluxes may have important implications for our understanding of C dynamics across the land-to-ocean continuum.

Catchment characteristics such as hydraulic gradient, vegetation cover, and soil moisture modulate the magnitude and location of groundwater discharge, while external factors like precipitation also influence discharge patterns (Leith et al., 2015; Olid et al., 2022), which in turn introduces spatial and temporal variability in both groundwater CO_2 inputs and their subsequent fate (i.e. emission vs. export). Heterogeneity in groundwater flow paths may explain the patchiness observed in CO_2 emissions, as well as variability in the fraction of CO_2 transported downstream along stream reaches (Hotchkiss et al., 2015a; Ledesma et al., 2018; Lupon et al., 2019). Although some studies support the significance of terrestrial CO_2 inputs via groundwater to stream CO_2 dynamics, most evidence remains indirect. Only a few studies have quantified the magnitude of groundwater CO_2 inputs to streams (Avery et al., 2018; Biehler et al., 2023; Call et al., 2018; Hotchkiss et al., 2015), and even fewer have examined their spatial and temporal variability (Lupon

https://doi.org/10.5194/egusphere-2025-5892
Preprint. Discussion started: 6 February 2026

et al., 2019), limiting our ability to understand the patterns and processes that control CO_2 dynamics in stream networks.

Various methods have been used to estimate groundwater inflow rates to streams, including temperature profiling (Briggs et al., 2012; Westhoff et al., 2011), electrical conductivity (Baxter et al., 2003), stream gauging (Cook, 2015; Schmadel et al., 2010), seepage meters (Boyle, 1994, Libelo & MacIntyre, 1994), and mass balance approaches (Rasilo et al., 2017; Rosenberry, 2008). However, these techniques often rely on simplifying assumptions and lack the resolution needed to capture the spatial and temporal variability of groundwater contributions. In contrast, dynamic assessments over days to weeks are possible through the natural radionuclide radon (^{222}Rn), which has gained recognition as a powerful tracer for quantifying groundwater-surface water exchange due to its high enrichment in groundwater, conservative behaviour, and short half-life ($T_{1/2}$ = 3.8 days) (Adyasari et al., 2023; Burnett et al., 2001). These properties make ^{222}Rn particularly well-suited for detecting fine-scale variability in groundwater inflows and their potential role in stream CO_2 dynamics. Nonetheless, studies explicitly linking ^{222}Rn-based groundwater inflow estimates to CO_2 emissions or downstream C export remain scarce and are often limited to short-term, low-flow conditions (Avery et al., 2018; Biehler et al., 2023; Call et al., 2018).

In this study, we investigated the role of groundwater inflow in regulating CO_2 emissions and downstream export in a boreal headwater stream. Using ^{222}Rn as a tracer, we assessed spatial and temporal patterns of groundwater inflow rates and associated CO_2 inputs during the ice-free period (from April to September). We hypothesized that groundwater inflow shapes CO_2 concentration patterns along the stream by acting as a direct source of CO_2. We expect a large fraction of terrestrial CO_2 delivered via groundwater to be rapidly emitted to the atmosphere upon entering the stream, but also a significant portion to be transported downstream. We further hypothesize that the influence of groundwater inflow on both stream CO_2 emissions and downstream export varies across space and time, likely driven by differences in topography and hydrological conditions.

2 Material and Methods

2.1 Study area

Our study focuses on Torrkälsbäcken, a headwater stream in northern Sweden (Fig. 1). The study region has a cold, humid boreal climate with a prolonged snow cover, typically lasting 167 days during the winter (1981-2015; Hjalmar Laudon & Ottosson Löfvenius, 2016). The average annual temperature recorded at the nearby Svartberget research station is 2.1 ºC (1986-2015), with a minimum of -8.6 ºC in January and a maximum of 14.6 ºC in July. The average annual precipitation is 619 mm, of which about 30% falls as snow (Hjalmar Laudon et al., 2021).

https://doi.org/10.5194/egusphere-2025-5892
Preprint. Discussion started: 6 February 2026

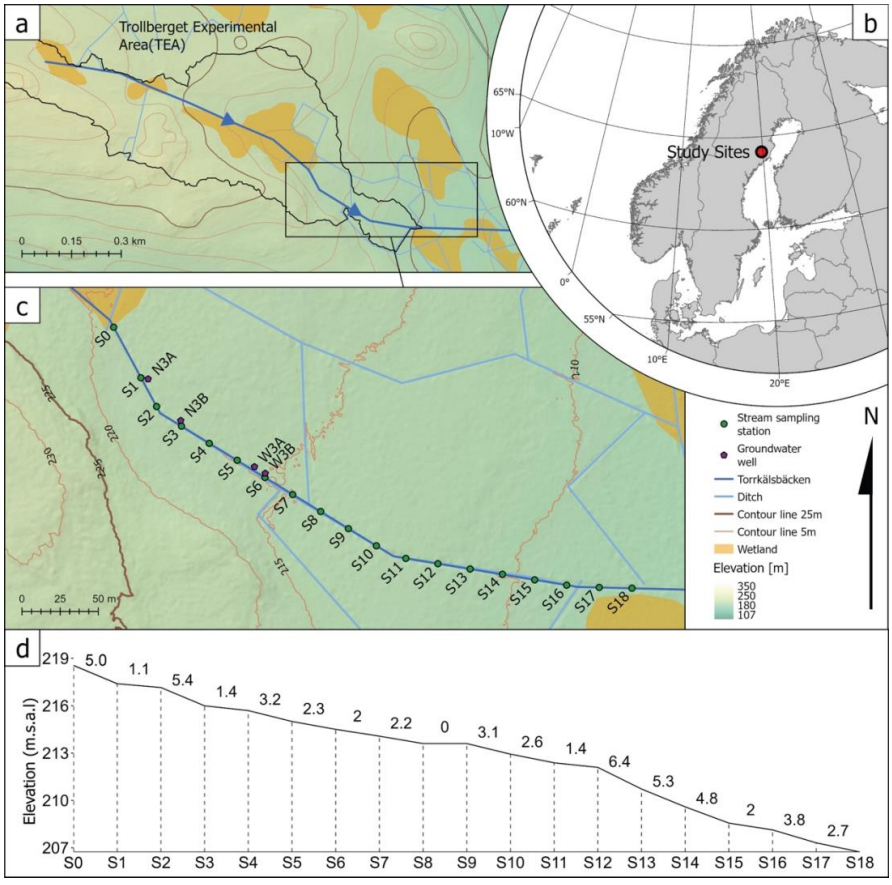

Figure 1: (a) Location of the Trollberget Experimetal Area (TEA), (b) a close-up of the study reach within TEA, (c) relative location within northern Europe and d) Elevation profile (in m) and slope (%) along the sampling stations of the stream (Hauptmann et al.,in revision). Locations of the outlet of an open mire (S0) and sampling stations (S1-S18) are shown in green circles. Locations of groundwater wells (G1, G3, G5, and G6) are shown in purple stars. Map created using *Terrangkartan* and 0.5 Digital Elevation Model (DEM). Data provided by Lantmäteriet (© Lantmäteriet).

Forest growing on podzol developed in glacial till covers 87% of the Torrkälsbäcken catchment area and consists mainly of Scots pine (*Pinus sylvestris* L.) and Norway spruce (*Picea abies* (L.) H. Karst.), also featuring birch (*Betula ssp.*), and scattered occurrences of alder (*Alnus incana* (L.) Moench), aspen (*Populus tremula* L.), and willow (*Salix spp.*) in the riparian areas. The remaining 13% of the catchment is covered equally by open mire and forest on mire. Torrkällsbäcken was ditch-trenched and straightened in the 1920s or 1930s to increase drainage

https://doi.org/10.5194/egusphere-2025-5892
Preprint. Discussion started: 6 February 2026

and hence timber production (Hasselquist et al., 2017; Norstedt & Laudon, 2019). This work introduced ditches as tributaries, affecting the hydrology of the stream (Fig. 1b). Since then, the stream has developed a riffle structure interspersed with occasional runs and step-pool systems. Pools and runs can reach wetted widths of up to 2 m, while riffle sections typically have an average width of 30 cm. The stream's hydrology is strongly influenced by snowmelt, resulting in peak water flows during spring flood, typically at the end of April (Laudon et al., 2013). Baseflow discharge varies between 0.5 and 2.0 L s^{-1} and is typical for the summer period (Hauptmann et al., in revision). A dense moss layer (*Polytrichum* spp. Hedw., *Sphagnum* spp. L.) predominates the ground vegetation alongside the stream within the channel, including areas that are periodically inundated, while dwarf shrubs (*Vaccinium myrtillus* L., *Vaccinium vitis-idaea* L.) dominate along the hillslope.

Our study quantified groundwater inflow rates and their influence on CO_2 emissions and export along a 400 m stretch of Torrkällsbäcken stream, beginning just downstream of a 2-ha open mire (Fig. 1b, S0) and continuing through forested podzol soil areas (Kuglerová et al., 2013; Laudon et al., 2020). The study reach comprises a transect of 18 sampling stations (S1–S18), where stations were distributed at 20 m intervals at elevations ranging from 207 to 219 m a.s.l., with slope differences between adjacent stations ranging from 0 to 6.4% (Fig. 1d). These topographic variations likely influence local hydrological conditions and vegetation distribution. The relatively even spacing of the stations enables detailed representation of these changes and allows comprehensive analysis of the effects of landscape heterogeneity on groundwater flow paths, inflow rates, and the associated input of CO_2 into streams.

2.2 Fieldwork and laboratory measurements

To cover seasonal variability under constraining hydrological conditions, stream water was sampled every second week from 24th of April to 23rd of September 2020, resulting in 13 sampling campaigns. During each campaign, stream stations were sampled on the same day, progressing from downstream to upstream. Samples were collected within a three-hour window (10:00 – 13:00h) to minimise the potential influence of the time of day.

For CO_2 analysis, 4 mL of stream water was sampled just below the water surface and injected into 22 mL gastight, acid-washed glass vials that had been flushed with N_2 at atmospheric pressure and spiked with 20 µL of 4% HCl to convert all inorganic C species to CO_2 (Klaus et al., 2018). The vial headspace was analysed for CO_2 partial pressure using a gas chromatograph (GC) (Clarus 500, PerkinElmer Inc., USA). Gas mixtures containing known concentrations of CO_2 (410 and 9400 ppm) were prepared, stored, and analysed alongside each batch of samples as standards. Triplicate samples of the standards yielded gas partial pressures within a 2% coefficient of variation. The measured headspace partial pressures (ppm) were converted to molar concentrations

https://doi.org/10.5194/egusphere-2025-5892
Preprint. Discussion started: 6 February 2026

according to the ideal gas law, Henry's law and the temperature-dependent solubility of CO_2 (Klaus et al., 2018). As sample acidification shifts the carbonate equilibrium towards CO_2, some of the measured headspace CO_2 may have resulted from other inorganic C species in the sample water. Therefore, we calculated the original CO_2 concentration in the water from the measured vial headspace CO_2 concentration using carbonate equilibrium reaction equations that account for the effects of pH and water temperature (Stumm & Morgan, 1995). On average, we found that 98.2 ± 0.7% of the dissolved inorganic C (DIC) was present in the form of CO_2 at an average pH of 4.7 ± 1.0 (Hauptmann et al., in revision). The detection limit for DIC was 0.3 µM, based on the water-headspace volume ratio used.

For ^{222}Rn concentrations, stream water samples were collected just below the water surface into 2-L polyethene terephthalate (PET) soda bottles using a submersible pump to minimize water-air contact and prevent ^{222}Rn degassing, while avoiding headspace. Once in the laboratory, ^{222}Rn concentrations in the stream water were measured using a Durridge Inc. RAD7 electronic radon-in-air monitor, which was coupled with the RAD7 soda bottle aerator kit accessory. In a closed-loop system, air was bubbled through the water samples for 40 minutes to reach equilibrium and the ^{222}Rn concentration was quantified through 15 counting cycles, each lasting 10 minutes. Simultaneously, water sample temperature was measured and recorded to determine the air-water partition coefficient. The ^{222}Rn in the water was then calculated from the measured ^{222}Rn concentration in the air. This calculation considered the volumes of air and water in the system, the water temperature during the measurement, the ambient ^{222}Rn concentration in the air, and the partitioning of ^{222}Rn between air and water. The calculation also adjusted for water temperature (Schubert et al., 2012). Additionally, corrections were made for the radioactive decay occurring between the sampling and the subsequent analysis of ^{222}Rn concentrations.

Groundwater (n = 56) was collected in eight PVC wells (Unoson Environment AB, Mölnlycke, Sweden, 25x32 mm in diameter), installed approximately 3 m from the stream to characterize the regional aquifers. The wells were arranged in four nests at 47, 74, 139, and 147 m (G1, G3, G5, and G6, respectively) from the uppermost stream segment close to the mire (see Fig. 1b). Each nest contained two wells, with screenings in the bottom 10 cm, which allowed the inflow of relatively shallow (0.75 – 0.90 m) and deep (1.15 – 1.30 m) groundwater, representing the Bs and C horizon, respectively. The intakes were below the groundwater table throughout the sampling period (Klaus et al., 2024). The wells were flushed the day before sampling to ensure complete groundwater renewal. The groundwater was then pumped using a peristaltic pump and sampled as the surface water, as described above. For ^{222}Rn analysis, 10 mL of filtered (0.45 µm) groundwater was collected and transferred directly to 20 mL polyethylene vials prefilled with 10 mL of high-efficiency liquid scintillator cocktail (Cable & Martin, 2008). ^{222}Rn concentrations in groundwater were analysed using an ultra-low level liquid scintillation counter (Quantulus

https://doi.org/10.5194/egusphere-2025-5892
Preprint. Discussion started: 6 February 2026

1220) with alpha-beta discrimination counting (background of 0.02 – 0.07 cpm; efficiency of 3.0 ± 0.2). The count rate of the measured sample was calculated from the start of measurement, taking into account the half-life of ^{222}Rn. For groundwater CO_2 analyses, we followed the procedure described in detail by (Klaus et al., 2024). Briefly, 10 mL of soil air that was in equilibrium with the groundwater was sampled from gas-permeable soil gas probes installed at the same locations and depths as the groundwater well intakes. We injected the air into pre-evacuated glass vials and analysed the partial pressure of CO_2 using a gas chromatograph (Clarus 580, PerkinElmer Inc., USA). To characterise the concentration of the gas in the groundwater end-member, we selected groundwater samples collected under conditions where groundwater flow was directed towards the stream (n = 42). This selection ensures that the samples accurately represent the contribution of groundwater flow chemistry. We inferred the direction of groundwater flow using Darcy's law based on manual groundwater level measurements taken at each sampling occasion at the wells sampled for ^{222}Rn, and at additional wells located 3 m from the ^{222}Rn sampling wells, i.e. 6 m from the stream (Klaus et al. 2024).

Stream discharge was estimated at five stations (S0, S4, S8, S13, and S18) (Fig. 1b) based on salt slug injections (Hauptmann et al., in revision). For the intermediate stations, ordinary least squares (OLS) regression was used to estimate the downstream increase in discharge (Hauptmann et al., in revision). The gas transfer velocity *k* was estimated by recording ambient sound recorded 30 cm above the stream surface using a handheld stereo audio recorder (Tascam DR-05X, TEAC Corporation, Santa Fe Springs, CA, USA), in accordance with published methodology (Hauptmann et al., in revision; Klaus et al., 2019). Ancillary parameters, including water temperature (T), temperature-specific conductivity (SPC), and air pressure, were measured *in situ* at the five stations with salt slug injections using a calibrated handheld water monitor (Yellow Springs Instruments ProSolo, Xylem Inc., Washington, DC, USA). Stream water samples for pH were collected without air bubbles in PVC bottles and kept cold upon return to the laboratory. We measured the pH using a benchtop meter (Mettler Delta 340) fitted with a pH Sensor (InLab® Power electrode, Mettler Toledo, Columbus, Ohio, United States). The mean depth and width of the stream segments between the stations were determined by averaging three measurements taken with a meter rod.

In autumn 2019, bulk mineral soil samples were collected from the same depths as the groundwater well intakes at the groundwater well sites using the core method and a volumetric cylinder (200 cm^3). These samples were weighed and dried to calculate dry bulk density. We derived porosity from bulk density, assuming a solid mass density of 2.65 g cm^{-3}, as verified by the pycnometer method (Blake & Hartge, 1986). The remaining soil samples were reserved for incubation experiments (Chanyotha et al., 2014; Corbett et al., 1998) to determine the diffusive ^{222}Rn input from the underlying soil, as well as the ^{222}Rn concentration in the groundwater.

https://doi.org/10.5194/egusphere-2025-5892
Preprint. Discussion started: 6 February 2026

Sediment samples were placed in 0.5 L PET bottles containing a known volume of Milli-Q water. These bottles were then measured using a RAD7 electronic radon-in-air monitor coupled with a RAD7 soda bottle aerator kit accessory, which ran 48 two-hour cycles. The rate of ^{222}Rn diffusion from the sediment (F_{diff}) was derived from the linear gradient obtained by plotting ^{222}Rn concentrations in air against time for the first seven hours of the experiment (Chanyotha et al., 2014). To determine the ^{222}Rn concentration in groundwater, approximately 200 g of dry sediment was placed in 0.5 L PET bottles, and the remaining volume was filled with Milli-Q water. All bottles were hermetically sealed and stored for 21 days, being periodically shaken. The ^{222}Rn concentration in groundwater was calculated as:

$$C_{gw} = C_{incubation} \frac{R_{lab}}{R_{field}} \quad (1)$$

where C_{gw} is the measured ^{222}Rn concentration [Bq m^{-3}], and R_{lab} and R_{field} are ratios of volume of water to sediment in the bottle (lab) and in the field (which is function of the porosity), respectively (Stieglitz et al., 2013). These parameters were incorporated into the ^{222}Rn mass to estimate groundwater inflow rates discharging into the study stream (see section 2.3).

2.3 Groundwater inflow rates and associated inputs of CO_2

Quantitative estimates of groundwater inflow rates were based on solving a mass balance equation that considered all sources of ^{222}Rn (i.e., advective groundwater flow, diffusive flux from bottom sediments, and production by its parent nuclide ^{226}Ra) and all sinks (i.e., radioactive decay in the water column and losses to the atmosphere). In a continuous-flow aquatic system that is not significantly affected by tributaries and is in steady state, a one-dimensional (1-D) mass balance model for the input of ^{222}Rn concentration ([Bq m^{-3}]) along a stream reach Δx_i can be written as:

$$\frac{d}{dx}(Q_i C_i)\Delta x_i \approx Q_{i-1}C_{i-1} - Q_i C_i = Q_{gw,i}C_{gw,i} + F_{diff}A_i + \lambda V_i C_{Ra,i} - F_{atm}A_i - \lambda V_i C_i \quad (2)$$

where Q_{i-1} and Q_i are the stream discharge [m^3 d^{-1}] at the upstream and downstream end of the stream section i; C_{i-i} and C_i [Bq m^{-3}] are the ^{222}Rn concentrations in the upstream and downstream segment, respectively; $Q_{gw,\,i}$ [m^3 d^{-1}] is the advective groundwater inflow discharging to the studied stream section i; $C_{gw,i}$ [Bq m^{-3}] is the ^{222}Rn concentration in the groundwater; F_{diff} is the molecular diffusion flux of ^{222}Rn from underlying sediments [Bq m^{-2} d^{-1}]; $C_{Ra,i}$ [Bq m^{-3}] is the ^{226}Ra concentration in the stream segment; F_{atm} [Bq m^{-2} d^{-1}] is the ^{222}Rn degassing to the atmosphere; λ is the ^{222}Rn decay constant [d^{-1}]; and A_i [m^2] and V_i [m^3] are the area and the volume of the studied stream segment, respectively. We acknowledge that the hyporheic flux of ^{222}Rn was assumed to be primarily mixed with ^{222}Rn inputs from shallow groundwater in the floodplain. Consequently, hyporheic water exchange is included in the total groundwater inflow flux to the stream. Evaporative losses of ^{222}Rn were considered negligible due to their extremely low rate in comparison to the gas transfer velocity of ^{222}Rn (Cook, 2015).

https://doi.org/10.5194/egusphere-2025-5892
Preprint. Discussion started: 6 February 2026

Equation (1) was used to estimate the flux of ^{222}Rn supplied to the stream compartment via groundwater ($F_{gw,i} = Q_{gw,i}C_{gw,i}$ [Bq d^{-1}]). The uncertainties associated with $F_{gw,i}$ were estimated deterministically by propagating the uncertainties of the individual terms in Equation 1. Using measurements of groundwater endmembers, we converted the ^{222}Rn fluxes supplied by groundwater ($F_{gw,i}$) into specific groundwater discharge (q_{gw}, [m d^{-1}]) and volumetric discharge (Q_{gw}, [m^3 d^{-1}]) based on a Monte Carlo analysis. To achieve this, we generated 1000 $F_{gw,i}$ values for each stream segment based on a normal distribution and the calculated $F_{gw,i}$ and its uncertainty. Groundwater inflow rates ($Q_{gw,i}$) were then calculated by dividing the $F_{gw,i}$ values by the ^{222}Rn concentration in the groundwater ($C_{gw,i}$). In this study, we report specific groundwater inflow rates [m d^{-1}] instead of volumetric discharge [m^3 d^{-1}] to enable direct comparison across stream segments of varying sizes, as segment dimensions inherently influence volumetric discharge. Finally, groundwater inflow rates were converted to groundwater-derived inputs of CO_2 using the measured concentrations of CO_2 in the groundwater end-members. Negative values of groundwater inflow rates and CO_2 inputs were considered as zero. The variability of groundwater inflow rates and derived CO_2 inputs was assessed by calculating the coefficient of variation (CV).

2.4 Stream CO_2 emissions and downstream export

To evaluate the importance of groundwater inflows in controlling CO_2 dynamics in the stream, we quantified total CO_2 losses through the two primary pathways (atmospheric emission and downstream export) and compared the magnitude of these with the contribution of groundwater.

^{222}Rn and CO_2 emissions across the water-air interface ([Bq m^{-2} d^{-1}] for ^{222}Rn, [mg C m^{-2} d^{-1}] for CO_2) were estimated using Fick's first law of gas diffusion:

$$F_{atm} = k_{gas}\left(C_{gas,i} - C_{gas,air}\right) \quad (3)$$

where k_{gas} [m d^{-1}] is the gas transfer velocity for the corresponding gas at the measured temperature, $C_{gas.i}$ and $C_{gas.air}$ ([Bq m^{-3}] for ^{222}Rn, and [g C m^{-3}] for CO_2) are the measured gas molar concentrations in the stream, and the theoretical concentrations in the stream if it was in equilibrium with the atmosphere, respectively, determined with the Henry's constant ($C_{CO2,i}$ =17 µM at 20ºC). The concentration of ^{222}Rn in the air was ignored because it was at least one order of magnitude lower than in the stream and groundwater.

Gas transfer velocity (k_{gas}) was estimated using the empirical equation of Macintyre et al. (1995):

$$k_{gas} = k_{600}\left(\frac{Sc}{600}\right)^{-0.5} \quad (4)$$

where Sc is the Schmidt number for the corresponding gas at the specific temperature (Sc is divided by 600 to normalize to CO_2 at 20ºC) (Wanninkhof, 2014). This conversion accounts for the effects

https://doi.org/10.5194/egusphere-2025-5892
Preprint. Discussion started: 6 February 2026

of gas-specific diffusivity on air-water gas exchange but ignores the potential effects of gas solubility on bubble-mediated gas exchange. Solubility effects only occur under sufficiently long bubble residence times and were likely negligible in our stream as validated by previous work in stream channels with similar hydraulic conditions (Klaus et al., 2022).

The standardised gas exchange velocity (k_{600}) was inferred at each stream reach using sound spectral analysis (Klaus et al., 2019) from the sound pressure level spectrum caused by bubbles in riffles and steps. Continuous estimates of discharge (Q, [L s^{-1}]) were used to model continuous k_{600} based on the sampling station-specific linear relationship between Q and k_{600} (Hauptmann et al., in revision).

We calculated the downstream CO_2 export [g CO_2 m^{-2} d^{-1}] for each stream segment by multiplying the discharge rate by the concentration of CO_2 at the downstream end of the stream segment.

2.5 Statistics

The manuscript reports the median and the 25th and 75th percentiles of the estimated values for stream and groundwater CO_2 and ^{222}Rn concentrations, groundwater inflow rates, inputs of CO_2 through groundwater, downstream CO_2 export, and atmospheric CO_2 emissions. Differences in gas concentrations between water sources (stream and groundwater), and spatial and seasonal variations in gas concentrations and fluxes were analysed using analysis of variance (ANOVA), followed by the Tukey-Kramer HSD post hoc test to identify differences between groups. Data were $\log_{10}$-transformed where necessary to meet assumptions of normality and homoscedasticity. Test results were considered statistically significant at $p < 0.05$. All analyses were conducted using the package 'stats' in R software (version 2023.12.1+402; R Core Team, 2023).

3 Results

3.1 Stream discharge and geochemical properties

3.1.1 Stream discharge

Measurements of stream discharge covered a wide range of hydrological conditions from the snowmelt period (April and May) to summer base flow (July and August), including rain events in July (see Appendix, Fig. S1). During the study period, discharge obtained through manual measurements (April-May) varied from 0.80 to 41 L s^{-1} (median 2.6 L s^{-1}, interquartile range (IQR): 1.4 – 13 L s^{-1}). Base-flow conditions were observed in mid-June and late August, with a median discharge of 1.29 L s^{-1} (IQR: 1.23 – 1.39 L s^{-1}). As indicated by elevated groundwater levels (Fig. S1b), high-flow conditions prevailed in early May, with a discharge peak of 37.5 L s^{-1} (IQR: 36.4 – 38.1 L s^{-1}). Elevated groundwater levels in July and August also reflected a secondary discharge peak at the end of July (13.4 L s^{-1}, IQR: 12.6 – 14.0 L s^{-1}), associated with rain events (Fig. S1c).

https://doi.org/10.5194/egusphere-2025-5892
Preprint. Discussion started: 6 February 2026

3.1.2 Stream geochemical properties

Throughout the season and across all stations, the stream was CO_2 supersaturated relative to the atmosphere (Fig. 2a). Concentrations of CO_2 in the stream ranged from 54 to 450 µM (174 µM, IQR: 145 – 214 µM). Maximum CO_2 concentration was found upstream (S1), adjacent to the mire (329 µM, IQR: 231 – 376 µM). Subsequently, CO_2 concentrations decreased downstream until reaching almost constant values at the downstream stations (S14 and S15: 138 µM, IQR: 125 – 150 µM). In the lowermost section of the studied stream reach, CO_2 concentrations increased slightly (S16- S18: 152 µM, IQR: 138 – 184 µM).

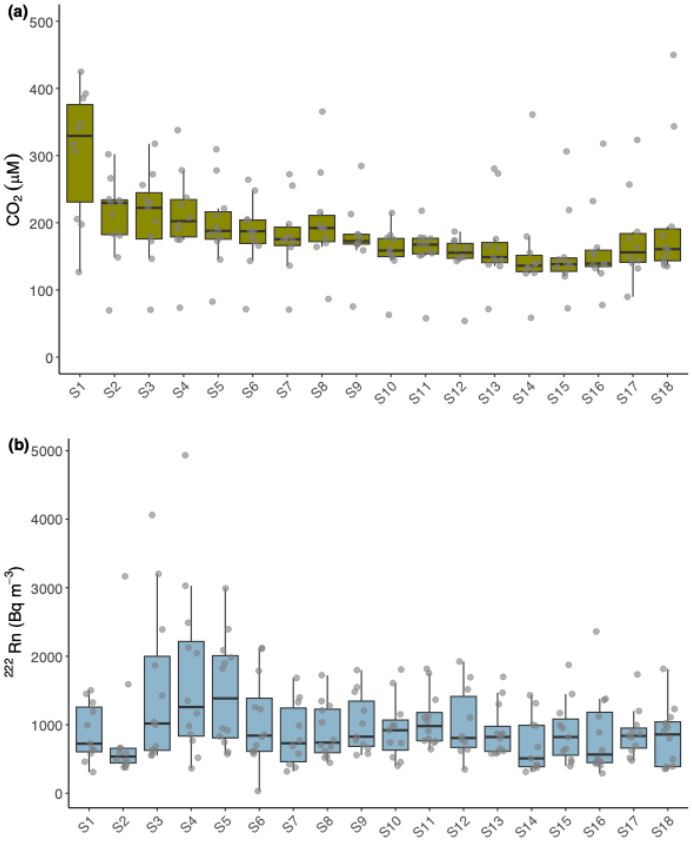

Figure 2: Boxplots showing concentrations of (a) CO_2 [µM] and (b) ^{222}Rn [Bq m^{-3}] along the stream reach. Each box represents the interquartile range (IQR), spanning from the 25th to the 75th percentile, with the solid line inside the box indicating the median value. Whiskers extend

https://doi.org/10.5194/egusphere-2025-5892
Preprint. Discussion started: 6 February 2026

to the most extreme data points within 1.5 times the IQR from the upper and lower quartiles. All individual observations used to construct the boxplots are plotted as grey circles.

The concentrations of ^{222}Rn in the stream water ranged from 32 to 4934 Bq m^{-3} (827 Bq m^{-3}, IQR: 581 – 1311 Bq m^{-3}) (Fig. 2b). The ^{222}Rn concentration increased slightly in the stream between stations S1 and S4, reaching a maximum of 1259 Bq m^{-3} (IQR: 835 – 2216 Bq m^{-3}). Downstream of station S4, the concentration of ^{222}Rn decreased and stabilised at a constant value of 827 Bq m^{-3} (IQR: 590 – 1229 Bq m^{-3}) along the studied stream reach. Over time, concentrations of ^{222}Rn correlated with CO_2 concentrations at the highest (S1 – S5) ($p < 0.041$, $R^2 = 0.37 – 0.65$) and lowest (S15 – S18) stream segments ($p < 0.04$, $R^2 = 0.39$ - 0.61) (Fig. S2), suggesting a consistent relationship between these two variables across different stream locations and conditions.

During the study period, we observed high temporal variability in CO_2 and ^{222}Rn concentrations in the stream water (Fig. 3). CO_2 concentrations were highest in early July (293 µM, IQR: 257 – 318 µM) and at the end of August (252 µM, IQR: 214 – 278 µM) (Fig. 3a). Similarly, ^{222}Rn concentrations were highest at the beginning of July (1816 Bq m^{-3}, IQR: 1631 – 2299 Bq m^{-3}), with a secondary peak at the end of August (1144 Bq m^{-3}, IQR: 936 – 1396 Bq m^{-3}) (Fig. 3b), concurrent with the peaks in CO_2 concentrations.

3.2 Groundwater geochemical properties

CO_2 concentrations in groundwater (1453 µM, IQR: 1202 – 1824 µM) were an order of magnitude higher than in stream water (Fig. S3a). A one-way ANOVA revealed a significant effect of well on CO_2 ($F = 3.047$, $p = 0.0406$), with higher concentrations found in well G6 than in well G3. Wells G1 and G5 had intermediate concentrations, not differing significantly from either G6 or G3. Dissolved CO_2 in groundwater varied across months (ANOVA, $F = 3.11$, $p = 0.0154$, Fig. S3c). Concentrations were lowest in July (906 µM, IQR: 666 – 1257 µM), intermediate in spring (April and May: 1265 µM, IQR: 1142 – 1463 µM), and highest in late autumn (September-October: 1652 µM, IQR: 1470 – 2091 µM).

^{222}Rn concentrations in groundwater (3591 µM, IQR: 1660 – 5525 µM) were at least three times higher than the ^{222}Rn concentration in the stream (Fig. S3b). Concentrations of ^{222}Rn in groundwater were lower in G6 than in the other wells (ANOVA, $F = 4.818$, $p = 0.0088$). In contrast to CO_2, ^{222}Rn concentrations did not vary throughout the sampling season (ANOVA, $F = 1.182$, $p = 0.35$, Fig. S3d). The anomalously low ^{222}Rn concentrations in well G6, together with Darcy's law estimates, suggest stream water infiltration rather than groundwater discharge. We excluded this well from the analyses as it does not represent the groundwater source of the study stream.

https://doi.org/10.5194/egusphere-2025-5892
Preprint. Discussion started: 6 February 2026

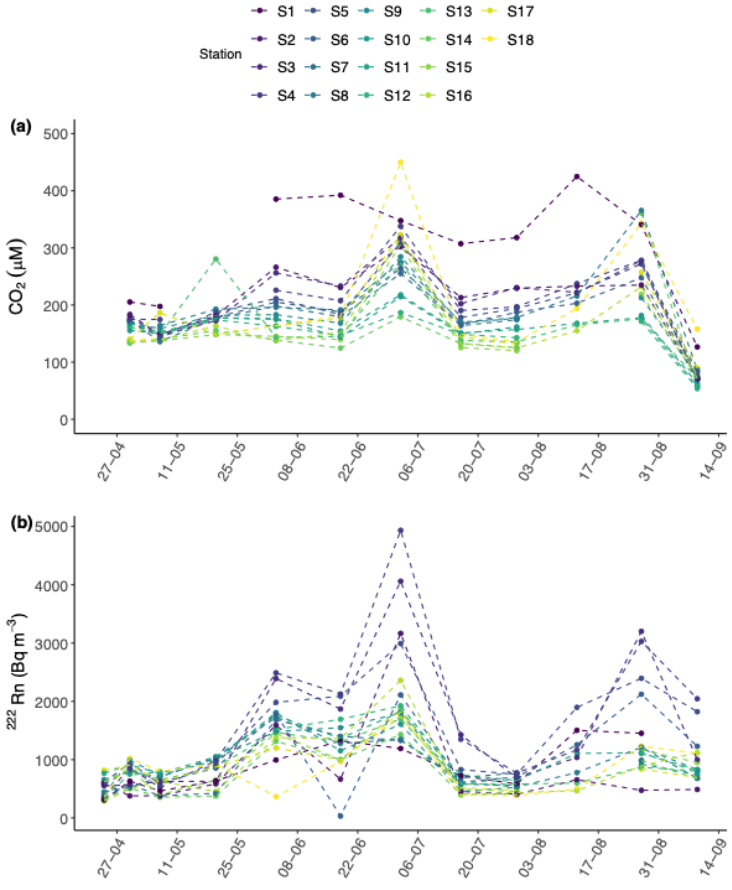

Figure 3: Temporal variation of (a) CO_2 and (b) ^{222}Rn concentration in the stream during the study period (dates shown as DD-MM). Different colors represent different stations.

3.3 Groundwater inflow rates and their significance to CO_2 emissions and export

3.3.1 Groundwater inflow rates

The rate at which groundwater flowed into the stream varied between different stream segments and at different times of the year, ranging from 0.00 to 31.5 m d^{-1} (0.281 m d^{-1}, IQR: 0.00 – 2.58 m d^{-1}) (Fig. 4). For comparison purposes, the groundwater flux estimated from the difference in discharge between upstream and downstream stations ($Q_i - Q_{i-1}$) ranged from 0.245 to 5.12 m d^{-1}. Notably, the median inflow derived from the ^{222}Rn mass balance (0.281 m d^{-1}) was close to the lower bound of the discharge-based estimates (0.245 m d^{-1}). This alignment with the minimum

https://doi.org/10.5194/egusphere-2025-5892
Preprint. Discussion started: 6 February 2026

value reflects the conservative nature of our methodology. Assuming an average stream width of 36 cm and a length of 20 m per stream segment, the average groundwater discharge rate corresponds to a volumetric flux of 2.02 m^3 d^{-1}, which is at the lower end of the range obtained from the discharge data (IQR: 1.63 – 11.7 m^3 d^{-1}).

We identified three distinct segments along the stream with significant groundwater inputs (S1-S4, S8-S11 and S14-S18, see Fig. 4a). These segments were classified as gaining reaches when the estimated groundwater flow (Q_{gw}) was positive, so that only net groundwater inflows were considered. In this way, the selected segments represent areas with consistently high groundwater inflows. The upstream segment (S1-S4) recorded the highest groundwater inflow rates, with a median value of 1.66 m d^{-1} (IQR: 0.00 – 5.29 m d^{-1}). Station S2 showed the highest groundwater inflow rate, with 7.69 m d^{-1} (IQR: 3.74 – 10.6 m d^{-1}). The intermediate (S8 – S11) and downstream (S14 – S18) segments showed lower groundwater contributions, with inflow rates of 0.350 m d^{-1} (IQR: 0.00 – 1.97 m d^{-1}) and 1.01 m d^{-1} (IQR: 0.225 – 2.62 m d^{-1}), respectively. Conversely, stream segments S5-S7 and S12-S13 showed no detectable groundwater inflows during most sampling campaigns. Spatial patterns in groundwater inflow rates suggest a dependence on landscape characteristics, particularly slope. Linear regression analysis revealed a significant relationship between groundwater inflow rates and slope at stations influenced by groundwater ($F = 5.372$, $p = 0.0407$), with slope explaining 33% of the variation in inflow rate (see Fig. S4).

The upstream segment S1-S4 exhibited a median value of CV of 135%, whereas the intermediate (S8-S11) and downstream (S14-S18) segments showed higher variability, with respective CVs of 167% and 183%. These relatively high CV values reflect the temporal variability of groundwater contribution across all segments. Similarly, individual stations showed a wide range of variability: S2 and S10 had the lowest CVs (74% and 95%, respectively), while S1, S9, and S15 had the highest (197%, 198%, and 240%, respectively). Despite differences in median groundwater inflow rates, the consistently high CVs across sections and stations indicate that, although recurrent, groundwater inputs were subject to strong temporal fluctuations throughout the sampling period. At the stations where groundwater inflows were detectable, we observed a trend towards higher values in May, with groundwater inflows of 2.24 m d^{-1} (IQR: 0.00778 – 4.88 m d^{-1}, Fig. 4b). A secondary increase in groundwater inflow rates was observed at the end of July and the beginning of August, with values of 0.44 m d^{-1} (IQR: 0.00 – 2.86 m d^{-1}).

https://doi.org/10.5194/egusphere-2025-5892
Preprint. Discussion started: 6 February 2026

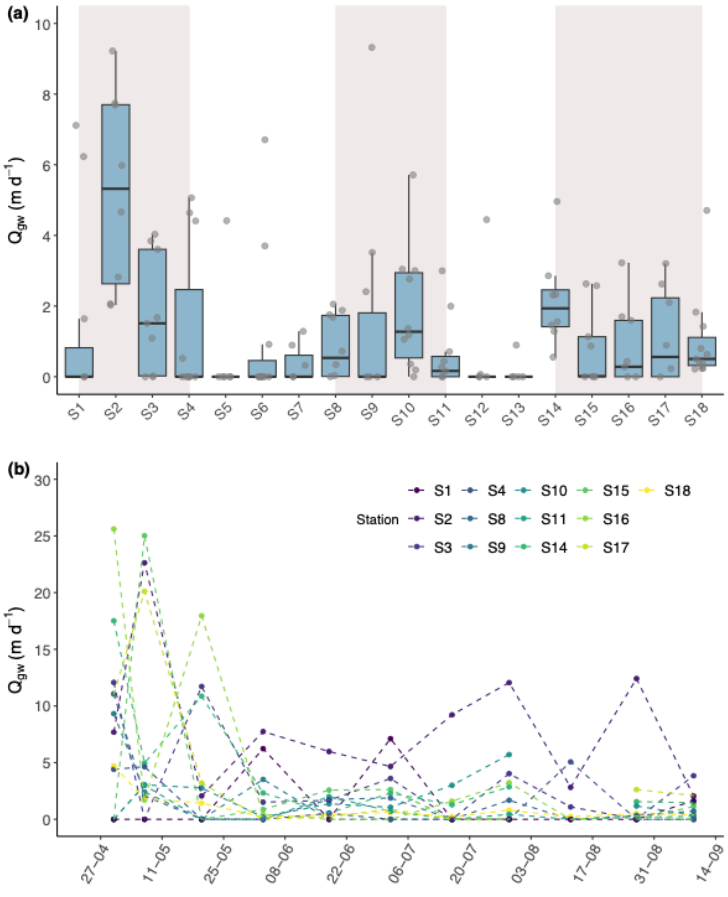

Figure 4: (a) Groundwater inflow rates along the stream reach. Each box represents the interquartile range (IQR), spanning from the 25th to the 75th percentile. The the solid line inside the box indicates the median value. Whiskers extend to the most extreme data points within 1.5 times the IQR of the upper and lower quartiles. The shaded areas indicate stations where groundwater inflows were notably present. All individual observations used to construct the boxplots are plotted as grey circles. (b) Temporal variations in the groundwater inflow rates at stations with significant groundwater inflow; dates are shown in DD-MM format.

406

407 **3.3.2 Stream CO_2 emissions and CO_2 downstream export**

408 The stream consistently emitted CO_2 into the atmosphere (Fig. 5a), with emissions ranging
409 from 0.3 to 25.1 g C m^{-2} d^{-1} (3.0 g C m^{-2} d^{-1}, IQR: 1.9 – 4.9 g C m^{-2} d^{-1}) across all stations and
410 throughout the study period. The highest CO_2 emissions were found at the topmost station (S1),
411 with 18.6 g C m^{-2} d^{-1} (IQR: 17.9 – 21.9 g C m^{-2} d^{-1}). Moderately elevated CO_2 emissions were

https://doi.org/10.5194/egusphere-2025-5892
Preprint. Discussion started: 6 February 2026

found at S2 and S16, with 7.4 g C m^{-2} d^{-1} (IQR: 6.4 – 8.5 g C m^{-2} d^{-1}) and 5.6 g C m^{-2} d^{-1} (IQR: 3.7 – 8.8 g C m^{-2} d^{-1}), respectively. A gradual decline in CO_2 emissions was observed from S2 to S10, followed by a subsequent increase in CO_2 emissions from S11 to S16. Further downstream of station S16, CO_2 emissions decreased again, reaching 2.2 g C m^{-2} d^{-1} (IQR: 2.1 – 2.6 g C m^{-2} d^{-1}) at the most downstream station (S18).

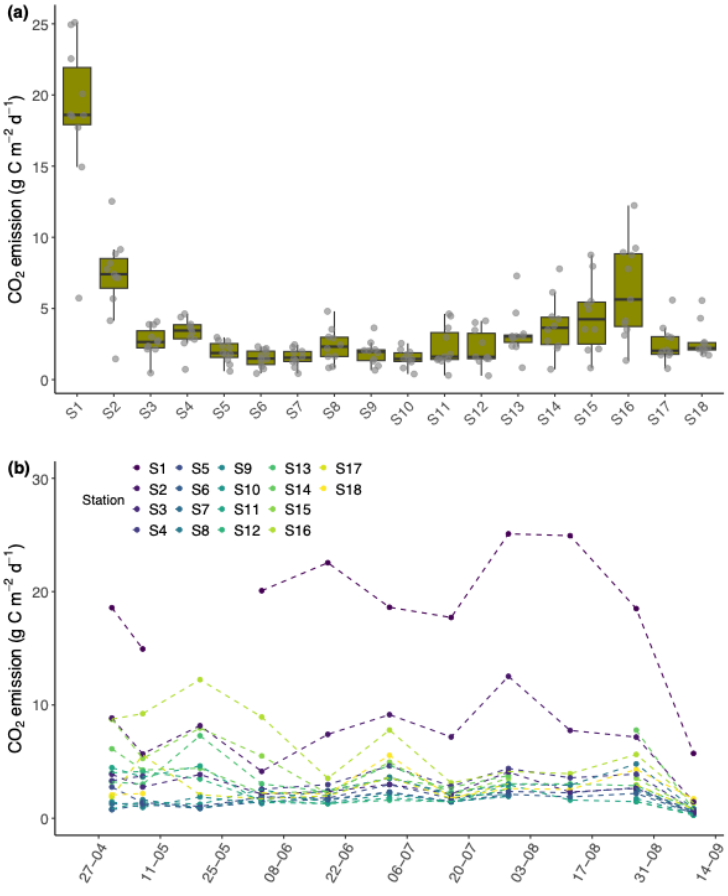

Figure 5: (a) Atmospheric emissions of CO_2 along the stream reach. Each box represents the interquartile range (IQR), spanning from the 25th to the 75th percentile, with the solid line inside the box indicating the median value. Whiskers extend to the most extreme data points within 1.5 times the IQR from the upper and lower quartiles. All individual observations used to construct the boxplots are plotted as grey circles. (b) Atmospheric emissions of CO_2 through the sampling season at the different stream segments.

https://doi.org/10.5194/egusphere-2025-5892
Preprint. Discussion started: 6 February 2026

CO_2 emissions were relatively stable throughout the sampling period, with consistently high emissions from late April to mid-August (2.6 g C m^{-2} d^{-1}, IQR: 1.9 – 4.1 g C m^{-2} d^{-1}) (Fig. 5b). Afterwards, a notable decline in CO_2 emissions was observed, with a tendency of values in September being lower (0.7 g C m^{-2} d^{-1}, IQR: 0.4 – 0.8 g C m^{-2} d^{-1}) than earlier in the year.

Downstream CO_2 export ranged from 9.2 to 864 g C m^{-2} d^{-1} (Fig. 6a). The median value for all stream segments was similar ($F = 0.03$, $p = 1$), at 76 g C m^{-2} d^{-1}. Downstream CO_2 export fluctuated throughout the sampling season (Fig. 6b). During base-flow conditions between mid-June and mid-July, CO_2 export varied from 28 to 92 g C m^{-2} d^{-1} (43 g C m^{-2} d^{-1}, IQR: 38 – 53 g C m^{-2} d^{-1}). The highest amounts of CO_2 were exported downstream in early May, with a median value of 647 g C m^{-2} d^{-1} (IQR: 611 – 678 g C m^{-2} d^{-1}). A second peak in downstream CO_2 export was observed at the end of July, with a median value of 330 g C m^{-2} d^{-1} (IQR: 296 – 355 g C m^{-2} d^{-1}).

3.3.3. Groundwater CO_2 inputs to the stream

For stream segments with significant groundwater inflows, the CO_2 input via groundwater ranged from 0.00 to 535 g C m^{-2} d^{-1} (Fig. 7a). The median groundwater CO_2 inputs (13 g C m^{-2} d^{-1}, IQR: 0.00 – 50 g C m^{-2} d^{-1}) exceeded the median atmospheric CO_2 emissions from these stream segments (3.0 g C m^{-2} d^{-1}, IQR: 1.9– 4.9 g C m^{-2} d^{-1}) by up to a factor of 20. Groundwater-derived CO_2 inputs were of the same order of magnitude as the CO_2 exported downstream (76 g C m^{-2} d^{-1}, IQR: 46– 300 g C m^{-2} d^{-1}). This suggests that a substantial proportion of the CO_2 delivered by groundwater is transported downstream rather than being emitted into the atmosphere.

Groundwater CO_2 inputs showed strong temporal variability (Fig. S5). The highest CO_2 inflows were observed at the end of April, reaching a median value of 108 g C m^{-2} d^{-1} (IQR: 58 – 126 g C m^{-2} d^{-1}). Inputs decreased towards the beginning of summer, but increased again in late July, reaching a median value of 136 g C m^{-2} d^{-1} (IQR: 46 – 175 g C m^{-2} d^{-1}). During baseflow conditions, groundwater CO_2 inputs were consistently low, with median values of 10 g C m^{-2} d^{-1} (IQR: 7.1 – 18 g C m^{-2} d^{-1}) in mid-July and 16 g C m^{-2} d^{-1} (IQR: 6.6 – 31 g C m^{-2} d^{-1}) in late August.

The relative contribution of groundwater-derived CO_2 inputs to stream CO_2 export, reported as the median across stations for each sampling date, varied markedly over time (Fig. 7b). The highest contribution occurred in early September, with groundwater CO_2 inputs accounting for up to 100% of the total downstream CO_2 export. Substantial contributions were also observed during baseflow conditions in summer, with groundwater accounting for 44% and 23% of the total CO_2 export in mid-June and late August, respectively.

https://doi.org/10.5194/egusphere-2025-5892
Preprint. Discussion started: 6 February 2026

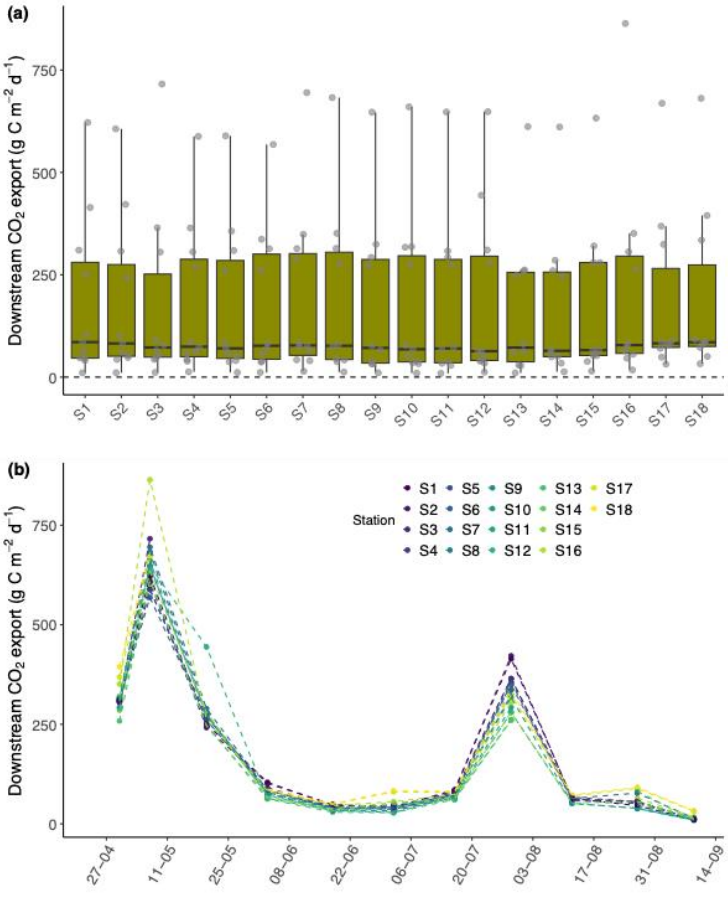

Figure 6: (a) Downstream CO_2 export across stream segments. Each box represents the interquartile range (IQR), spanning from the 25th to the 75th percentile, with the solid line inside the box indicating the median value. Whiskers extend to the most extreme data points within 1.5 times the IQR from the upper and lower quartiles. All individual observations used to construct the boxplots are plotted as grey circles. (b) Stream CO_2 export through the sampling season.

451

452

https://doi.org/10.5194/egusphere-2025-5892
Preprint. Discussion started: 6 February 2026

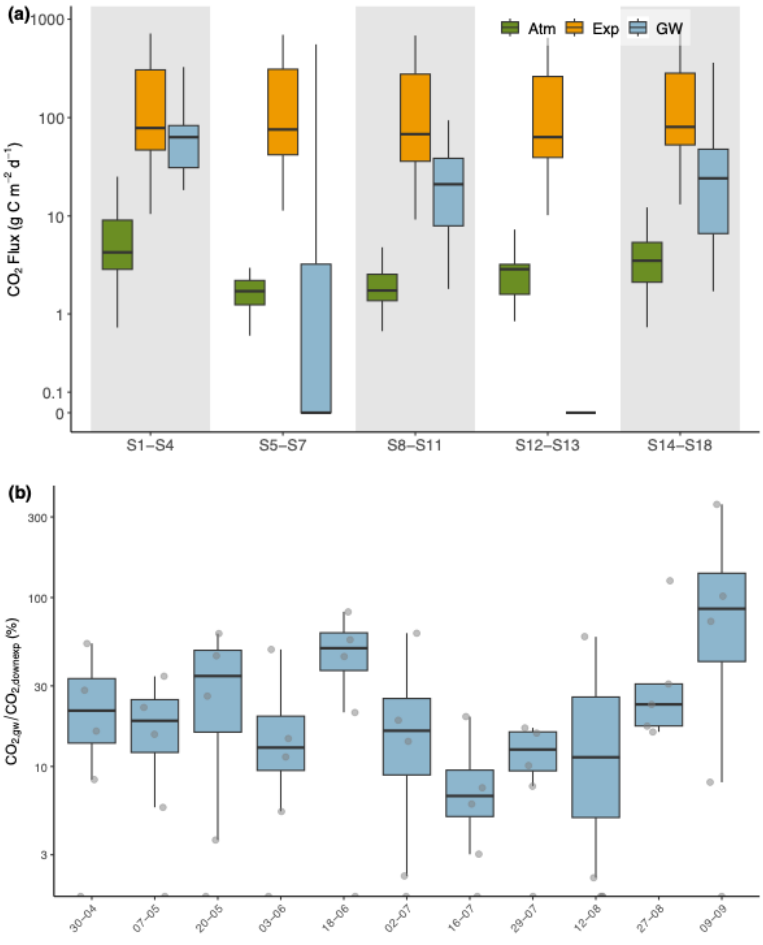

Figure 7. CO_2 fluxes in stream segments shown on a logarithmic scale. (a) Comparison of CO_2 fluxes via groundwater, atmospheric emissions, and downstream export. (b) Temporal variation in the relative contribution of groundwater CO_2 inputs to downstream CO_2 export along the stream. Each box represents the interquartile range (IQR), spanning from the 25th to the 75th percentile, with the solid line inside the box indicating the median value. Whiskers extend to the most extreme data points within 1.5 times the IQR from the upper and lower quartiles. All individual observations used to construct the boxplots in panel b) are plotted as grey circles.

4 Discussion

4.1 Spatio-temporal variations of groundwater CO_2 inputs to boreal headwater streams

4.1.1 Spatial variations in groundwater CO_2 inputs

https://doi.org/10.5194/egusphere-2025-5892
Preprint. Discussion started: 6 February 2026

Groundwater CO_2 inputs to the study stream showed spatial variability at the scale of tens of meters (Fig. 7a), which is consistent with previous observations in nearby boreal streams (Lupon et al., 2019b). However, after excluding one hydrogeochemically distinct well (identified a priori by an anomalous ^{222}Rn signature), CO_2 concentrations did not differ significantly among wells (Fig. S3a). This indicates that the observed spatial heterogeneity is more likely driven by differences in groundwater inflow rates rather than by variation in riparian CO_2 production. This interpretation is further supported by the positive correlation between CO_2 and ^{222}Rn concentrations in both upstream (S1 – S5) and downstream (S15 – S18) stations (Fig. S2), which highlights the effectiveness of ^{222}Rn as a tracer of groundwater-derived CO_2 inputs. The observed spatial variability in groundwater inflows significantly affects reach-scale estimates of CO_2 evasion (Hotchkiss et al., 2015a; Lupon et al., 2019), emphasizing the need to account for such heterogeneity when quantifying stream C fluxes.

Spatial patterns in groundwater inflow rates appear to depend on landscape characteristics, particularly slope. Steeper areas tend to have higher inflow rates, likely due to stronger hydrological gradients promoting infiltration and subsurface channel flows (Leach et al., 2017; McGlynn & McDonnell, 2003). This pattern is further supported by the positive correlation observed between slope and groundwater inflow rates at high-inflow stations (see Fig. S4). In contrast, lower inflow rates were associated to more gentle slopes, highlighting the role of topography in shaping groundwater contributions to streams. This finding corroborates previous research on the role of groundwater inflows in groundwater-dependent ecosystems, suggesting that higher rates of groundwater typically occur where rivers or streams run adjacent to hills or flow through incised valleys (Cartwright & Gilfedder, 2015). However, the magnitude of groundwater inflows along the stream showed a considerable range of temporal variability as indicated by the coefficients of variation (CV). Notably, stream segments influenced by groundwater exhibited high CV values (~ 200%; S1, S8, S9, and S15), reflecting significant temporal fluctuations in groundwater inflows. This variability is likely caused by transient hydrological factors, including variable recharge rates, preferential flow paths, localized aquifer heterogeneities, and human impact such as ditching (Fig. 1b). These factors can cause groundwater inflows to fluctuate in magnitude and timing, which would increase the CV. Heterogeneity in groundwater inflows along the stream reach was also reflected in differences in water table depth among the monitoring wells (Fig. S1b), with mean depths varying up to a factor of four between wells. Together, these observations emphasize the spatial and temporal complexity of hydrological pathways and groundwater dynamics, highlighting the need for site-specific studies to more accurately capture the contribution of groundwater to stream CO_2 emissions.

Variations in soil composition along the stream reach may influence the availability of CO_2 for groundwater export, potentially contributing to the observed spatial patterns of groundwater

https://doi.org/10.5194/egusphere-2025-5892
Preprint. Discussion started: 6 February 2026

CO_2 inputs. Autotrophic root respiration and heterotrophic respiration of organic C stored in the riparian zone are recognised as the main sources of soil CO_2 and lateral transport to the stream (Campeau et al., 2019; Hope et al., 2004). In our study, however, we did not detect clear differences in CO_2 concentrations between groundwater wells, likely because the monitoring network had limited spatial coverage, being confined to ~ 200m of the stream corridor. A denser network of groundwater wells would be needed to better resolve potential small-scale heterogeneity in subsurface CO_2 production and transport along the stream corridor.

4.1.2 Temporal variations in groundwater CO_2 inputs

While spatial variability shaped the distribution of groundwater CO_2 inputs along the stream, temporal fluctuations were equally important in determining the magnitude and timing of these inputs. The highest groundwater CO_2 inputs were observed in late spring (late April- early May) (Fig. S5), with median values exceeding CO_2 emissions to the atmosphere (Fig. 5a). These peaks in groundwater CO_2 inputs were mainly caused by increased groundwater inflow rates driven by snowmelt (Fig. 4a) (Audrey Campeau et al., 2014; Dyson et al., 2011), rather than by elevated CO_2 concentrations in the groundwater. Reduced respiration during winter likely limited the accumulation of dissolved CO_2 in the groundwater, as reflected by the lower CO_2 concentrations found in May compared to those in summer and early autumn (Klaus et al., 2024) (Fig. S3c). Therefore, although snowmelt is usually linked with low CO_2 concentrations in groundwater, the substantial increase in water table levels and inflow rates during this period means that groundwater is a significant pathway for lateral CO_2 transfer. This emphasizes the need to consider not only CO_2 concentrations, but also hydrological dynamics when evaluating the role of groundwater in stream C cycling.

CO_2 inputs via groundwater were also relatively high in late summer and early autumn (Fig. S5), which coincided with precipitation events and associated increased stream discharge (see Fig. S1). This pattern is consistent with previous observations showing that intensive rainfall events recharge the groundwater system and enhance interactions between groundwater and surface water, likely through rapid infiltration and increased hydraulic connectivity between the aquifer and the stream. Groundwater recharge raises the water table (see Fig. S1b), thereby increasing the hydraulic head gradient between the groundwater and the stream. This, in turn, drives higher groundwater inflow rates (Cartwrigth & Gilfedder 2015) and reinforces the strong hydrological coupling between surface water and groundwater in the study area. Additionally, higher soil temperatures in summer compared to spring (Klaus et al., 2024) may accelerate the decomposition of soil organic matter, thereby increasing the production of dissolved OC (DOC) in soil porewater (Schelker et al., 2013). Root respiration during periods of peak primary production also contributes to elevated CO_2 concentrations in soil and groundwater (Högberg et al., 2001). Together, these processes may explain the higher CO_2 concentrations observed in groundwater during late summer

https://doi.org/10.5194/egusphere-2025-5892
Preprint. Discussion started: 6 February 2026

and autumn (Fig. S3c). The combination of elevated soil and groundwater CO_2 concentrations, alongside significant groundwater inflow following summer and early autumn rainfall events, results in substantial CO_2 inputs to the stream via groundwater. This mechanism is modulated by physical factors, such as stream morphology, sediment permeability, and precipitation, as well as biological factors such as primary production. Therefore, understanding these interactions is critical to understanding the role of groundwater in shaping CO_2 dynamics in headwater streams. This highlights the importance of considering not only hydrological processes, but also biological processes, when studying CO_2 production and export within the catchment, as these may vary over time.

4.2 The magnitude and fate of groundwater CO_2 inputs

We consistently observed higher CO_2 concentrations in groundwater than in stream water, which supports our hypothesis that groundwater inflows can serve as an important source of CO_2 to headwater streams under conditions favouring subsurface transport. Similar CO_2 enrichments have been reported in the riparian groundwater of other boreal forests (Biehler et al., 2023; Lupon et al., 2019; Venkiteswaran et al., 2014). Groundwater CO_2 concentrations at our study site were consistent with (Venkiteswaran et al., 2014, Klaus et al. 2018) or at the upper end of those reported in nearby catchments (Lupon et al., 2019). These findings suggest that relatively small groundwater inflows can disproportionately impact a stream's CO_2 budget.

Results from the ^{222}Rn mass balance indicate that groundwater inflow from the riparian zone primarily occurred at three main segments along the stream reach (see A4A). CO_2 inputs at these segments highlight the role of groundwater as a significant source of C to headwater streams, with inputs exceeding total CO_2 emissions by up to 20-fold (Fig. 7a). Median groundwater CO_2 input is comparable to values reported for a nearby catchment during the ice-free period (Lupon et al., 2019). These findings highlight the importance of groundwater for stream C budgets, particularly in systems with spatially focused inflows. While a portion of this CO_2 is likely evaded shortly after entering the stream (Öquist et al., 2009), the magnitude of inputs relative to emissions emphasizes that groundwater can substantially sustain in-stream CO_2 availability.

Not all CO_2 delivered via groundwater is immediately emitted to the atmosphere. A substantial fraction may be transported downstream (Hauptmann et al., in revision), where it can either contribute to CO_2 emissions further along the network or be utilized in in-stream processes (Hotchkiss et al., 2015). When averaged over the entire sampling season and limited to stream segments influenced by groundwater inflows, these inputs accounted for up to 100% of the total downstream CO_2 export. High-resolution spatial and temporal sampling revealed substantial variability, with up to a three-fold difference among stream segments and a ten-fold variation

https://doi.org/10.5194/egusphere-2025-5892
Preprint. Discussion started: 6 February 2026

across sampling dates, highlighting the dynamic and localized role of groundwater in shaping stream C fluxes.

5 Conclusions

This study highlights the critical role of groundwater inflow in transferring terrestrially derived CO_2 into boreal headwater streams and shaping stream C dynamics. While not all groundwater-derived CO_2 is immediately released into the atmosphere, our results indicate that a substantial fraction is transported downstream, where it can fuel further emissions along the stream continuum or be used in in-stream biological processes. The fate of this CO_2 (rapid atmospheric evasion, downstream export, or in-stream processing) depends on hydrological and biogeochemical controls, including gas exchange velocity, water depth, and travel time. Spatially, contributions from groundwater vary markedly at fine spatial scales (tens of meters) and are shaped by catchment characteristics such as stream slope, with additional modulation by preferential flow paths, localised aquifer heterogeneities, or variable recharge. Temporally, groundwater CO_2 inputs are regulated by hydrological processes (snow melt- and rainfall- driven recharge) and biological activity (e.g., soil respiration), which together control the production and transport of CO_2 from the riparian zone to the stream. Comprehensive assessments of the patterns and controls of stream CO_2 dynamics therefore require an evaluation of both the spatial and temporal variability of groundwater inflows, as well as downstream export, atmospheric emission, and biological activity, not only within the channel but also throughout the riparian corridor. This integrative understanding is particularly important in the context of global environmental change, as it improves our ability to predict how boreal headwater streams will respond to changing climate and hydrological conditions

6 Supplement

The supplement used in this article are publicly available at the Figshare Digital Repository via the following link: https://doi.org/10.6084/m9.figshare.30501437 (Olid et al., 2025).

7 Author contribution

Conceptualization and methodology by DH, MK, JK, and CO; investigation and data curation by CO, DH and MK; formal analysis by CO; funding acquisition by JK, MK, and CO; resources by JK, MK and CO; visualization by CO and DH; writing – original draft preparation by CO; writing – review and editing by DH, MK, JK, and CO.

8 Competing interests

The authors declare that they have no competing interests.

9 Acknowledgements

https://doi.org/10.5194/egusphere-2025-5892
Preprint. Discussion started: 6 February 2026

We acknowledge the assistance in the field and laboratory from Erik Geibrink and Anders Jonsson at Umeå University. We also thank Morgan Karlsson, Christer Moreira Boman, and Hassan Ridha for their assistance with installing the groundwater well and soil gas probe infrastructure, and Valenti Rodellas for his help with ^{222}Rn analyses and his valuable comments and constructive feedback. We acknowledge the Krycklan Catchment Study and the Swedish Infrastructure for Ecosystem Science (SITES) for access to the sites and precipitation data, and the Biogeochemical Analytical Facility (BAF) at Umeå University for chemical analysis.

10 Financial support

This study was financially supported by FORMAS (Grants no. 2018-01217 and 2018-00885) with a grant awarded to CO and JK, and Stiftelsen Skogssällskapet (grant number 2019-657-Steg 2 2018) and The Geological Survey of Sweden (grant number 36–2788/2021) with grants awarded to MK. CO acknowledges financial support from the Spanish Ministry of Science, Innovation and Universities through the PERMAFLOW project (PID2023-148093NB-I00).

11 References

Adyasari, D., Dimova, N. T., Dulai, H., Gilfedder, B. S., Cartwright, I., McKenzie, T., and Fuleky, P.: Radon-222 as a groundwater discharge tracer to surface waters, Earth Sci. Rev., 238, 104321, https://doi.org/10.1016/j.earscirev.2023.104321, 2023.

Ågren, A., Berggren, M., Laudon, H., and Jansson, M.: Terrestrial export of highly bioavailable carbon from small boreal catchments in spring floods, Freshwater Biol., 53, 964–972, https://doi.org/10.1111/j.1365-2427.2008.01955.x, 2008.

Avery, E., Bibby, R., Visser, A., Esser, B., and Moran, J.: Quantification of Groundwater Discharge in a Subalpine Stream Using Radon-222, Water, 10, 100, https://doi.org/10.3390/w10020100, 2018.

Balathandayuthabani, S., Panneer Selvam, B., Gålfalk, M., Saetre, P., Peura, S., Kautsky, U., Klemedtsson, L., Arunachalam, L., Vellingiri, G., Bastviken, D.: Methane in Two Stream Networks: Similar Contributions From Groundwater and Local Sediments While Oxidation Was a Large Sink Controlling Atmospheric Emissions, J. Geophys. Res.: Biogeosci., 129, e2023JG007836, https://doi.org/10.1029/2023JG007836, 2024.

Baxter, C., Hauer, F. R., and Woessner, W. W.: Measuring Groundwater–Stream Water Exchange: New Techniques for Installing Minipiezometers and Estimating Hydraulic Conductivity, Trans. Am. Fish. Soc., 132, 493–502, https://doi.org/10.1577/1548-8659(2003)132<0493:MGWENT>2.0.CO;2, 2023.

https://doi.org/10.5194/egusphere-2025-5892
Preprint. Discussion started: 6 February 2026

628 Biehler, A., Buffin-Bélanger, T., Baudron, P., and Chaillou, G.: Groundwater discharge
629 contribution to dissolved inorganic carbon and riverine carbon emissions in a subarctic region.
630 Biogeochemistry, 165, 129–150, https://doi.org/10.1007/s10533-023-01060-9, 2023.

631 Blake, G., and Hartge, H.: Bulk density, In Methods of Soil Analysis, Part 1 - Physical and
632 Minerological Methods (2nd edition) (pp. 363–382), American Society of Agronomy - Soil
633 Science Society of America, Madison, 1986.

634 Boyle, D. R.: Design of a seepage meter for measuring groundwater fluxes in the nonlittoral zones
635 of lakes-Evaluation in a boreal forest lake. Limnol. Oceanogr., 39, 670–681,
636 https://doi.org/10.4319/lo.1994.39.3.0670, 1994.

637 Briggs, M. A., Lautz, L. K., and McKenzie, J. M.: A comparison of fibre-optic distributed
638 temperature sensing to traditional methods of evaluating groundwater inflow to streams, Hydrol.
639 Processes, 26, 1277–1290, https://doi.org/10.1002/hyp.8200, 2012.

640 Burnett, W. C., Lambert, M., and Dulaiova, H.: Tracing groundwater discharge into the ocean via
641 continuous radon-222 measurements. MTS/IEEE Oceans 2001. An Ocean Odyssey. Conference
642 Proceedings (IEEE Cat. No.01CH37295), Honolulu, HI, USA, 2001, pp. 251-255 vol.1, https://doi:
643 10.1109/OCEANS.2001.968734, 2001.

644 Cable, J. E., and Martin, J. B.: In situ evaluation of nearshore marine and fresh pore water transport
645 into Flamengo Bay, Brazil, Estuarine Coastal Shelf Sci., 76, 473–483,
646 https://doi.org/10.1016/J.ECSS.2007.07.045, 2008.

647 Call, M., Sanders, C. J., Enrich-Prast, A., Sanders, L., Marotta, H., Santos, I. R., and Maher, D. T.:
648 Radon-traced pore-water as a potential source of CO2 and CH4 to receding black and clear water
649 environments in the Amazon Basin, Limnol. Oceanogr. Lett., 3, 375–383,
650 https://doi.org/10.1002/lol2.10089, 2018.

651 Campeau, A., Bishop, K., Amvrosiadi, N., Billett, M. F., Garnett, M. H., Laudon, H., Öquist, M.G.,
652 Wallin, M.B.: Current forest carbon fixation fuels stream CO2 emissions, Nat. Commun., 10, 1876,
653 https://doi.org/10.1038/s41467-019-09922-3, 2019.

654 Campeau, Audrey, Lapierre, J. F., Vachon, D., and Del Giorgio, P. A.: Regional contribution of
655 CO2 and CH4 fluxes from the fluvial network in a lowland boreal landscape of Québec, Global
656 Biogeochem. Cycles, 28, 57–69, https://doi.org/10.1002/2013GB004685, 2014.

657 Cartwright, I., and Gilfedder, B.: Mapping and quantifying groundwater inflows to Deep Creek
658 (Maribyrnong catchment, SE Australia) using 222Rn, implications for protecting groundwater-
659 dependant ecosystems, Appl. Geochem., 52, 118–129,
660 https://doi.org/10.1016/j.apgeochem.2014.11.020, 2015.

https://doi.org/10.5194/egusphere-2025-5892
Preprint. Discussion started: 6 February 2026

Chanyotha, S., Kranrod, C., abd Burnett, W. C.: Assessing diffusive fluxes and pore water radon activities via a single automated experiment, J. Radioanal. Nucl. Chem., 301, 581–588, https://doi.org/10.1007/s10967-014-3157-3, 2014.

Cook, P. G.: Quantifying river gain and loss at regional scales, J. Hydrol., 531, 749–758. https://doi.org/10.1016/j.jhydrol.2015.10.052, 2015.

Corbett, D. R., Burnett, W. C., Cable, P. H., and Clark, S. B.: A multiple approach to the determination of radon fluxes from sediments, J. Radioanal. Nucl. Chem., 236, 247–253, https://doi.org/10.1007/BF02386351, 1998.

Drake, T. W., Raymond, P. A., and Spencer, R. G. M.: Terrestrial carbon inputs to inland waters: A current synthesis of estimates and uncertainty, Limnol. Oceanogr. Lett., 3, 132–142. https://doi.org/10.1002/lol2.10055, 2018.

Dyson, K. E., Billett, M. F., Dinsmore, K. J., Harvey, F., Thomson, A. M., Piirainen, S., and Kortelainen, P.: Release of aquatic carbon from two peatland catchments in E. Finland during the spring snowmelt period, Biogeochemistry, 103, 125–142, https://doi.org/10.1007/s10533-010-9452-3, 2011.

Hauptmann, D., Klaus, M., Sponseller, R. A., Olid, C., Laudon, J., and Karlsson, J. Discharge modulates the dominance of downstream carbon export over evasion in a boreal headwater stream. In Revision.

Högberg, P., Nordgren, A., Buchmann, N., Taylor, A. F. S., Ekblad, A., Högberg, M. N., Nyberg, G., Ottosson-Löfvenius, M., and Read, D.D.: Large-scale forest girdling shows that current photosynthesis drives soil respiration, Nature, 411, 789–792, https://doi.org/10.1038/35081058, 2001.

Hope, D., Palmer, S. M., Billett, M. F., and Dawson, J. J. C.: Variations in dissolved CO2 and CH4 in a first-order stream and catchment: an investigation of soil–stream linkages, Hydrol. Processes, 18(17), 3255–3275, https://doi.org/10.1002/hyp.5657, 2004.

Hotchkiss, E. R., Hall Jr, R. O., Sponseller, R. A., Butman, D., Klaminder, J., Laudon, H., Rosvall, M., Karlsson, J.: Sources of and processes controlling CO2 emissions change with the size of streams and rivers. Nat. Geosci, 8, 696–699, https://doi.org/10.1038/ngeo2507, 2015.

Klaus, M., Geibrink, E., Hotchkiss, E. R., and Karlsson, J.: Listening to air-water gas exchange in running waters, Limnol. Oeanogr-Meth., 17, 395–414, https://doi.org/10.1002/lom3.10321, 2019.

Klaus, M., Labasque, T., Botter, G., Durighetto, N., and Schelker, J.: Unraveling the Contribution of Turbulence and Bubbles to Air-Water Gas Exchange in Running Waters, J. Geophys. Res-: Biogeosci., 127, e2021JG006520, https://doi.org/10.1029/2021JG006520, 2022.

https://doi.org/10.5194/egusphere-2025-5892
Preprint. Discussion started: 6 February 2026

694 Klaus, Marcus, Geibrink, E., Jonsson, A., Bergström, A.-K., Bastviken, D., Laudon, H.,
695 Klaminder, J., Karlsson, J.: Greenhouse gas emissions from boreal inland waters unchanged after
696 forest harvesting, Biogeosciences, 15, 5575–5594. https://doi.org/10.5194/bg-15-5575-2018,
697 2018.

698 Klaus, Marcus, Öquist, M., and Macháčová, K.: Tree stem-atmosphere greenhouse gas fluxes in a
699 boreal riparian forest. Sci. Total Environ., 954, 176243.
700 https://doi.org/10.1016/j.scitotenv.2024.176243, 2024.

701 Kuglerová, L., Nilsson, G., and Hasselquist, E. M.: Too much, too soon? Two Swedish case studies
702 of short-term deadwood recruitment in riparian buffers, Ambio, 52, 440-452,
703 https://doi.org/10.1007/s13280, 2023.

704 Laudon, H, Taberman, I., Ägren, A., Futter, M., Ottosson-Löfvenius, and Bishop, K. The Krycklan
705 catchment study - A flagship infrastructure for hydrology, biogeochemistry, and climate research
706 in the boreal landscape, Water Resour. Res., 49, 7154–7158. https://doi.org/10.1002/wrcr.20520,
707 2013.

708 Laudon, H., Maher Hasselquist, E., Peichl, M., Lindgren, K., Sponseller, R., Lidman, F.,
709 Kuglerová, L., Hasselquist, N.J., Bishop, K., Nilsson, M.B., Ågren, A. M.: Northern landscapes in
710 transition: Evidence, approach and ways forward using the Krycklan Catchment Study, Hydrol.
711 Processes, 35, e14170, https://doi.org/10.1002/hyp.14170, 2020.

712 Laudon, H. and Ottosson Löfvenius, M.: Adding snow to the picture – providing complementary
713 winter precipitation data to the Krycklan Catchment Study database, Hydrol. Processes, 30, 2413–
714 2416, https://doi.org/10.1002/hyp.10753, 2016.

715 Laudon, H., Hasselquist, E. M., Peichl, M., Lindgren, K., Sponseller, R., Lidman, F., Kuglerová,
716 L., Hasselquist, N.J., Bishop, K., Nilsson, M.B., Ågren, A.M.: Northern landscapes in transition:
717 Evidence, approach and ways forward using the Krycklan Catchment Study. Hydrological
718 Processes, 35(4). https://doi.org/10.1002/hyp.14170, 2021.

719 Leach, J. A., Lidberg, W., Kuglerová, L., Peralta-Tapia, A., Ågren, A. M., and Laudon, H.:
720 Evaluating topography-based predictions of shallow lateral groundwater discharge zones for a
721 boreal lake-stream system, Water Resour. Res, 53, 5420-5437, https://doi.org/10.1002/, 2017.

722 Ledesma, J. L. J., Futter, M. N., Blackburn, M., Lidman, F., Grabs, T., Sponseller, R. A., Laudon,
723 H., Bishop, K.J., and Köhler, J.: Towards an Improved Conceptualization of Riparian Zones in
724 Boreal Forest Headwaters, Ecosystems, 21, 297–315, https://doi.org/10.1007/s10021-017-0149-5,
725 2018.

726 Leith, F. I., Dinsmore, K. J., Wallin, M. B., Billett, M. F., Heal, K. V., Laudon, H., Öquist, M.G.,
727 Bishop, K.: Carbon dioxide transport across the hillslope–riparian–stream continuum in a boreal

https://doi.org/10.5194/egusphere-2025-5892
Preprint. Discussion started: 6 February 2026

headwater catchment, Biogeosciences, 12, 1881–1892, https://doi.org/10.5194/bg-12-1881-2015, 2015.

Li, M., Peng, C., Zhang, K., Xu, L., Wang, J., Yang, Y., Li, P., Liu, Z., and He N.: Headwater stream ecosystem: an important source of greenhouse gases to the atmosphere, Water Res., 190, 116738, https://doi: 10.1016/j.watres.2020.116738, 2021.

Libelo, E. L., and MacIntyre, W. G.: Effects Of Surface-Water Movement On Seepage-Meter Measurements Of Flow Through The Sediment-Water Interface, Hydrogeol. J., 2, 49–54. https://doi.org/10.1007/s100400050047, 1994.

Lupon, A., Denfeld, B. A., Laudon, H., Leach, J., Karlsson, J., and Sponseller, R. A.: Groundwater inflows control patterns and sources of greenhouse gas emissions from streams, Limnol. Oceanogr., 64, 1545–1557, https://doi.org/10.1002/lno.11134, 2019.

Lantmäteriet. GSD-Vegetationsdata (GSD vegetationdata, 2012).

Macintyre, S., Wanninkhof, R., and Chanton, J. P. Trace gas exchange across the air-water interface in freshwater and coastal environments. In Biogenic Trace Gases: Measuring emissions from soil and water (pp. 52-57.), 1995.

Maher Hasselquist, E., Lidberg, W., Sponseller, R. A., Ågren, A., and Laudon, H.: Identifying and assessing the potential hydrological function of past artificial forest drainage, Ambio, 47, 546–556, https://doi.org/10.1007/s13280-017-0984-9, 2017.

McGlynn, B. L., and McDonnell, J. J.: Quantifying the relative contributions of riparian and hillslope zones to catchment runoff, Water Resour. Res., 39, 1310, https://doi.org/10.1029/2003WR002091, 2003.

Mwakanyamale, K., Slater, L., Day-Lewis, F., Elwaseif, M., and Johnson, C.: Spatially variable stage-driven groundwater-surface water interaction inferred from time-frequency analysis of distributed temperature sensing data, Geophys. Res. Lett., 39, L06401, https://doi.org/10.1029/2011GL050824, 2012.

Natchimuthu, S., Wallin, M. B., Klemedtsson, L., and Bastviken, D.: Spatio-temporal patterns of stream methane and carbon dioxide emissions in a hemiboreal catchment in Southwest Sweden. Sci. Rep., 7, 39729, https://doi.org/10.1038/srep39729, 2017.

Norstedt, G., and Laudon, H.: Krycklan: Markanvändning från forntid till nutid (in Swedish). Retrieved from https://pub.epsilon.slu.se/18715, 2019.

Olid, C., Rodellas, V., Rocher-Ros, G., Garcia-Orellana, J., Diego-Feliu, M., Alorda-Kleinglass, A., Bastviken, D., and Karlsson, J.: Groundwater discharge as a driver of methane emissions from Arctic lakes, Nat. Comm., 13, 3667, https://doi.org/10.1038/s41467-022-31219-1, 2022.

https://doi.org/10.5194/egusphere-2025-5892
Preprint. Discussion started: 6 February 2026

761 Olid, C., Karlsson, J., Klaus, M., Hauptmann, D.
762 GWinputs_Emissions_Export_of_CO2_in_a_boral_stream.figshare. Dataset.
763 http://doi.org/10.6084/m9.fisghare.30501437.vs, 2025.

764 Öquist, M. G., Wallin, M., Seibert, J., Bishop, K., and Laudon, H.: Dissolved inorganic carbon
765 export across the soil/stream interface and its fate in a boreal headwater stream. Environ. Sci.
766 Technol., 43, 7364–7369. https://doi.org/10.1021/es900416h, 2009.

767 Rasilo, T., Hutchins, R. H. S., Ruiz-González, C., and del Giorgio, P. A.: Transport and
768 transformation of soil-derived CO2, CH4 and DOC sustain CO2 supersaturation in small boreal
769 streams, Sci. Total Environ., 579, 902–912, https://doi.org/10.1016/j.scitotenv.2016.10.187, 2017.

770 Raymond, P. A., Hartmann, J., Lauerwald, R., Sobek, S., McDonald, C., Hoover, M., Butman, D.,
771 Striegl, R., Mayorga, E., Humborg, C., Kortelainen, P., Dürr, H., Meybeck, M., Ciais, P., and Guth,
772 P.: Global carbon dioxide emissions from inland waters, Nature, 503, 355–9,
773 https://doi.org/10.1038/nature12760, 2013.

774 R Core Team: R: A language and environment for statistical computing. R Foundation for
775 Statistical Computing. Retrieved from http://www.R-project.org/, 2017.

776 Rosenberry, D. O.: A seepage meter designed for use in flowing water. J. Hydrol., 359, 118–130,
777 https://doi.org/10.1016/j.jhydrol.2008.06.029, 2008.

778 Schelker, J., Grabs, T., Bishop, K., and Laudon, H.: Drivers of increased organic carbon
779 concentrations in stream water following forest disturbance: Separating effects of changes in flow
780 pathways and soil warming, J. Geophys. Res. Biogeosci. 118, 1814–1827,
781 https://doi.org/10.1002/2013JG002309, 2013.

782 Schmadel, N. M., Neilson, B. T., and Stevens, D. K.: Approaches to estimate uncertainty in
783 longitudinal channel water balances, J. Hydrol., 394, 357–369,
784 https://doi.org/10.1016/j.jhydrol.2010.09.011, 2010.

785 Schubert, M., Paschke, A., Lieberman, E., & Burnett, W. C.: Air-water partitioning of 222Rn and
786 its dependence on water temperature and salinity, Environ. Sci. Technol., 46, 3905–3911.
787 https://doi.org/10.1021/s204680n, 2012.

788 Stanley, E. H., Loken, L. C., Casson, N. J., Oliver, S. K., Sponseller, R. A., Wallin, M. B., Zhang,
789 L., and Rocher-Ros, G.: GRiMeDB: the Global River Methane Database of concentrations and
790 fluxes, Earth Syst. Sci. Data, 15, 2879–2926, https://doi.org/10.5194/essd-15-2879-2023, 2023.

791 Stieglitz, T. C., Beek, P., Souhaut, M., and Cook, P. G.: Karstic groundwater discharge and
792 seawater recirculation through sediments in shallow coastal Mediterranean laggons, determined

https://doi.org/10.5194/egusphere-2025-5892
Preprint. Discussion started: 6 February 2026

from water, salt and radon budgets, Mar. Chem., 156, 73–84, https://doi.org/10.1016/j.marchem.2013.05.005, 2013.

Stumm, W., and Morgan, J. J.: Aquatic Chemistry: Chemical Equilibria and Rates in Natural Waters (Vol. 10: 0471511854). ISBN 0471511854, 9780471511854.: Wiley., 1995.

Venkiteswaran, J. J., Schiff, S. L., and Wallin, M. B.: Large Carbon Dioxide Fluxes from Headwater Boreal and Sub-Boreal Streams, PLoS One, 9, e101756, https://doi.org/10.1371/journal.pone.0101756, 2014.

Wallin, M. B., Campeau, A., Audet, J., Bastviken, D., Bishop, K., Kokic, J., Laudon, H., Lundin, E., Löfgren, S., Natchumuthu, S., Sobek, S., Teutschbein, C., Weyhenmeyer, G.A., Grabs, T.: Carbon dioxide and methane emissions of Swedish low-order streams—a national estimate and lessons learnt from more than a decade of observations, Limnol. Oceanogr. Lett., 3, 156–167, https://doi.org/10.1002/lol2.10061, 2018.

Wanninkhof, R.: Relationship between wind speed and gas exchange over the ocean revisited, Limnol. Oceanogr. Methods, 12, 351–362, https://doi.org/10.4319/lom.2014.12.351, 2014.

Westhoff, M. C., Bogaard, T. A., and Savenije, H. H. G.: Quantifying spatial and temporal discharge dynamics of an event in a first-order stream, using distributed temperature sensing, Hydrol. Earth. Syst. Sci., 15, 1945–1957. https://doi.org/10.5194/hess-15-1945-2011, 2011.